

Protein Crystallization from a Preordered Metastable Intermediate Phase Followed by Real-Time Small-Angle Neutron Scattering

Ralph Maier, Benedikt Sohmen, Stefano Da Vela, Olga Matsarskaia, Christian Beck, Ralf Schweins, Tilo Seydel, Fajun Zhang,* and Frank Schreiber



Cite This: *Cryst. Growth Des.* 2021, 21, 6971–6980



Read Online

ACCESS |



Metrics & More

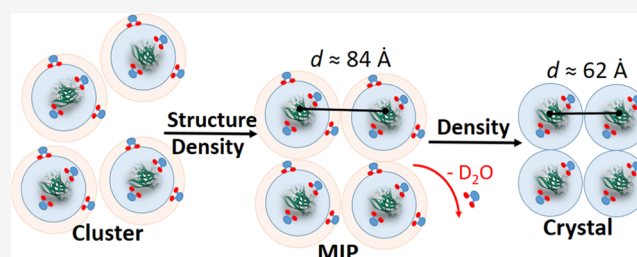


Article Recommendations



Supporting Information

ABSTRACT: We present a systematic study using real-time small-angle neutron scattering (SANS) and optical microscopy to follow the protein crystallization process in the presence of a metastable intermediate phase (MIP). Using bovine β -lactoglobulin (BLG) in the presence of the divalent salt CdCl_2 as a model system, we first determine the experimental phase behavior in D_2O . The protein solutions become turbid after crossing the first threshold salt concentration c^* , and upon further increasing the salt concentration, the solutions become less turbid but not completely clear again. Thus, the second border is called pseudo- c^{**} . Near pseudo- c^{**} , crystallization follows a nonclassical process with a MIP, which is further explored with a focus on the structural evolution and the growth kinetics of the MIP prior to crystal nucleation. Real-time SANS measurements show that a correlation peak develops inside the MIP, and its peak position shifts to higher q -values with time, finally stabilizing at a characteristic length scale of $d_{\text{MIP}} \approx 84$ Å. The area of this peak (proportional to the amount of MIP in the sample) increases with time first, reaches a maximum, and then decreases quickly upon crystallization due to consumption by crystal growth. The evolution of the correlation peak indicates a “preordering” nature of the MIP as precursors of crystal nucleation, which lowers the nucleation barrier for subsequent crystallization. These results of structural evolution and the role of MIPs during a nonclassical crystallization process may be relevant for other fields ranging from structural biology to pharmacy.



INTRODUCTION

Crystallization, especially of proteins, is important not only for structural biology, where high-quality crystals are required for structure determination, but also in research areas like pharmacological drug delivery, where protein crystals are used for stability reasons while simultaneously allowing for a controlled drug release in the body.^{1,2} However, the molecular interactions in protein solutions and their connections to the crystallization process are not fully understood and crystal growth is typically performed by screening several conditions and optimizing those which result in protein crystals.³

The early stage of crystallization, i.e., the nucleation process, is often interpreted following classical nucleation theory (CNT).^{4,5} One of the main assumptions of CNT is that molecules form nuclei in a supersaturated solution with the exact density and structure of the crystals in the final stage.^{6–8} Recent studies in protein and colloid crystallization as well as biomineralization have shown nonclassical features in the early stage of nucleation.^{6,9–30} Hence, according to the nonclassical nucleation theory, a metastable intermediate phase (MIP) (clusters or dense liquid phases) exists in between the initial solution and the final crystalline state.^{6,9,10,12,31} The free energy landscapes of nonclassical pathways show an additional local

free energy minimum corresponding to this intermediate phase.²³

In the nonclassical nucleation theory, the order parameters, i.e., density and structure, are decoupled. In most studies, the liquid precursors gain higher density prior to reaching their final structure.^{9,10,13,32–35} Nevertheless, also the scenario of preordered MIPs serving as a nucleation precursor was reported.^{23,36,37} One example is the solid–solid transformation from an initially formed polymorph toward a more stable crystal structure, where the less stable crystals serve as preordered precursors.^{38–41} Another example is the so-called “oriented attachment” in crystallization, in which building blocks (which might be crystalline or not) form independently and then attach to the crystal surface in the required orientation, forming mesocrystals in the case of crystalline precursors.^{42–47}

Received: August 9, 2021

Revised: October 16, 2021

Published: October 29, 2021



In solution crystallization, preordered precursors have been observed for small molecules, colloids, as well as for protein systems.^{30,35,37,43,48–51} For minerals such as calcium carbonate (CaCO_3), a partial dehydration of the prenucleation clusters was found to be crucial for liquid–liquid phase separation (LLPS) and further solidification.^{30,35} A different nature of additives (such as polyaspartic acid or magnesium) can lead to different types of short-range order within the amorphous precursors.⁴⁸ In a second step, water is expelled from these precursors, resulting in long-range order.⁴⁸ In simple aromatics (perylene diimides), cryogenic electron microscopy revealed an initial densification of the precursors, which is followed by a gradual evolution, involving further densification parallel to optimizing molecular order and morphology.⁵¹ Using cryo-scanning transmission electron microscope (STEM) tomography, also for proteins such as ferritin, a gradual increase in both order and density from the surface of the precursor toward their interior was recently reported.⁵² Despite the progress in two-step nucleation theory, its application and our understanding of the preordered precursors in terms of their structural development as well as the exact role in crystal nucleation are still elusive.^{29,36,46,53}

We have previously shown that trivalent salts such as YCl_3 or CeCl_3 can induce a reentrant condensation (RC) phase behavior in many acidic proteins like β -lactoglobulin (BLG) or human serum albumin (HSA).^{54–63} Interestingly, depending on the position in the phase diagram, classical crystallization or a nonclassical crystallization process have been observed.^{24–26,59} In a previous study,^{25,26} the two-step nucleation process of protein crystallization in solutions was investigated by following the overall crystallization kinetics using real-time optical microscopy and small-angle X-ray scattering (SAXS).^{25,26} For BLG-salt (CdCl_2) solutions in H_2O at the transition zone of pseudo- c^{**} , small aggregates formed after sample preparation. These protein aggregates were identified as a metastable intermediate phase (MIP) during crystallization. The experimental results together with a consistent rate equation model provided solid evidence of two-step nucleation in the early stage of crystallization.^{25,26} However, a detailed characterization of the MIP as a key ingredient in the crystallization and its evolution during crystallization is still missing.

In this work, we study BLG- CdCl_2 , which was previously studied in H_2O only, in heavy water (D_2O). Establishing D_2O as a solvent responds to the fundamental interest in associating the physical differences of D_2O and H_2O with differences in the resulting biological assembly. Moreover, it permits subsequent small-angle neutron scattering (SANS) experiments to investigate the structural evolution of the MIP during a two-step crystallization process, as well as subsequent neutron spectroscopy investigations to explore the diffusive protein dynamics in situ during the crystallization. In addition, NMR studies may be aided as well by establishing D_2O as a solvent.⁶⁴ In general, real-time scattering techniques provide information on the ensemble average and structural information with good statistics,^{24–26,65} which is in contrast to the real-space real-time techniques where details of the local domains of the system can be probed.^{47,66,67} SANS has the advantage of being a noninvasive method with a large scattering volume. These are crucial aspects regarding the crystallization of (biological) protein solutions in which the crystal number density may be very small. Hence, this real-time study not only provides direct evidence for a two-step

nucleation process but also elucidates the role and the structural signature of the MIP in the nonclassical process of protein crystallization.

EXPERIMENTAL SECTION

Materials and Sample Preparation. The protein β -lactoglobulin (BLG) from bovine milk, D_2O and the divalent salt CdCl_2 were purchased from Sigma-Aldrich (now Merck). For BLG (product no. L3908), a purity of $\geq 90\%$; for D_2O (product no. 151882), a purity of $\geq 99.9\%$; and for CdCl_2 (product no. 202908), a purity of $\geq 99\%$ were guaranteed. In all experiments of this study, D_2O was used as a solvent to obtain a good contrast in the neutron scattering experiments.

Stock solutions were prepared by dissolving the salt and protein powder, respectively, in D_2O . The protein concentration of the protein stock solutions was determined by UV–vis absorption measurements with an extinction coefficient of $0.96 \text{ mL}\cdot\text{mg}^{-1}\cdot\text{cm}^{-1}$ at a wavelength of 278 nm.⁶⁸ For sample preparation, appropriate amounts of D_2O , protein stock solution, and salt stock solution were mixed. In this work, the samples were prepared without additional buffer since buffers can affect the phase behavior of proteins and the solubility of salts. The pH values determined in H_2O were all in a range between 6 and 7. Using the relation $\text{pH}_{\text{D}_2\text{O}} = \text{pH}_{\text{H}_2\text{O}} + 0.4$,^{69,70} the pH values were well above the isoelectric point of BLG of 5.2.⁷¹ All experiments were performed at $20 \pm 1 \text{ }^\circ\text{C}$.

Optical Microscopy. Protein crystallization in real time was followed with an optical microscope (Axio Scope.A1, Carl Zeiss AG) in the bright-field mode. The samples were mixed in 1.5 mL plastic tubes (Sarstedt, Germany), directly transferred into a Gene Frame (1 cm \times 1 cm with a thickness of 0.25 mm and a volume of 25 μL from Thermo Scientific, Germany) on a glass slide and subsequently covered with a cover slide to prevent evaporation. Images were taken by the microscope-included camera Axio-Cam ICc5 (Carl Zeiss AG) in time intervals according to the time scale of the investigated crystallization process. Since we are interested in the evolution of the sample, the focus area was kept constant to monitor the same spot for a few days. The software ZEN Lite 2012 was used to conduct the imaging as well as to measure the crystal lengths.

Small-Angle Neutron Scattering (SANS). SANS measurements were carried out at beamline D11 at ILL, Grenoble, France.⁷² The advantages of SANS are the negligible radiation damage and the large scattering volume containing a large amount of sample material, which ensure a good statistical average. The sample-to-detector distance was set to 2 m, which covers a q -range from 0.03 to 0.33 \AA^{-1} at a wavelength of 6 \AA ($\Delta\lambda/\lambda = 10\%$). Protein-salt solutions in D_2O were filled in rectangular quartz cells with a path length of 2 mm. The beam size on the sample was 7 mm \times 10 mm and the acquisition time per run was 240 s. Runs were repeated in appropriate time intervals to follow the crystallization process over a period of 3 days. H_2O was used as a secondary standard to calibrate the absolute scattering intensity. Data were stored in NEXUS data format.⁷³ The data correction and absolute intensity calibration were obtained using the software LAMP.⁷⁴ A detailed data analysis was performed by MATLAB and will be described in more detail in the **Results and Discussion** section. Data can be accessed via refs 75 and 76.

RESULTS AND DISCUSSION

Experimental Phase Diagram of BLG with CdCl_2 in D_2O . We first present the phase diagram established in this context for the completely new system BLG with CdCl_2 in D_2O (see **Figure 1**) to obtain an overview of the phase behavior, which will be compared with the phase diagram in H_2O in previous work.^{25,26} Samples of different protein concentrations (c_p) and salt concentrations (c_s) were systematically prepared and probed for optical transmission. Depending on their grade of turbidity, they are assigned to regime I, II, or III. In regime I, the protein-salt solutions are clear, since the initially negatively charged proteins⁵⁵ repel each other and are

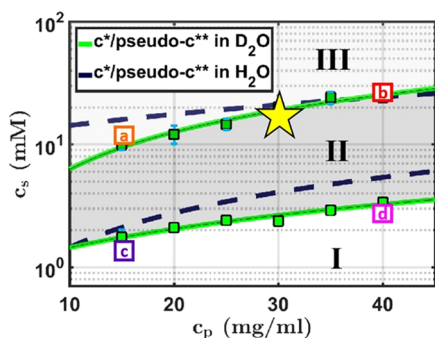


Figure 1. Experimental phase diagram of BLG with CdCl_2 in D_2O at 21°C . In regime I, the negatively charged proteins repel each other and the protein-salt solutions are clear. At $c_s > c^*$, they turn turbid due to the formation of aggregates (regime II). By further increasing c_s above pseudo- c^{**} , the turbidity decreases again, but does not vanish completely (regime III). In addition to the phase boundaries in D_2O , the phase boundaries in H_2O determined in our previous work are included as dashed lines.²⁴ The yellow star indicates the region selected for real-time SANS and optical microscopy experiments.

stable in solution. Upon increasing c_s above c^* , a first sharp transition occurs from a clear to a turbid solution and one enters a condensed regime, referred to as regime II. By increasing c_s even further, a second phase boundary referred to as pseudo- c^{**} is observed, above which the solutions become gradually less turbid (regime III).^{55,60} This phase behavior is denoted reentrant condensation (RC).^{54,55} In contrast to what is observed in the presence of trivalent ions, the transition from regime II to III is not sharp and the solutions do not become completely clear again in regime III. Therefore, the mean c_s of the last clear and first turbid or last turbid and first clearer sample is referred to as c^* or pseudo- c^{**} , respectively. If not smaller than the symbols, the blue error bars indicate the standard deviations (see Figure 1).

For comparison, the phase boundaries in H_2O determined in our previous work²⁴ are included (Figure 1, dashed lines). Using D_2O instead of H_2O , c^* is slightly shifted toward lower salt concentrations. This deviation becomes stronger for higher protein concentrations and indicates that protein–protein interactions are stronger and the system is more attractive.⁷⁷ However, a substantial broadening of regime II when H_2O is replaced by D_2O , as reported recently for bovine and human serum albumin solutions in the presence of trivalent ions, is not observed for BLG.^{62,77}

Crystallization was observed for samples in regime II. In agreement with our previous work, the resulting crystal morphology and growth kinetics depend strongly on the sample location in the phase diagram.^{24–26,59} Figure 2 shows representative crystal morphologies for the sample conditions labeled in the phase diagram (a–d). Crystals grown close to c^* show elongated, biccapped prism morphologies, whereas crystals grown at the pseudo- c^{**} boundary are more roundish and compact. Regarding crystallization kinetics in H_2O , close to c^* , crystallization follows a classical one-step pathway.^{24–26} Below pseudo- c^{**} , in regime II, an intermediate phase is observed before the crystals start to grow.^{25,26} Note that Cd^{2+} cations were previously found to improve protein crystal size, morphology, and diffraction quality.^{78,79} For this system, however, all crystals are twin crystals and therefore the structural elucidation is more challenging.

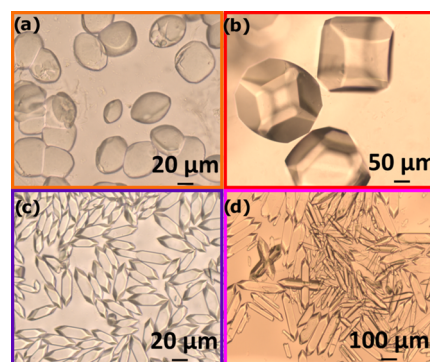


Figure 2. Different crystal morphologies depending on the location in the phase diagram as indicated in Figure 1: (a) 15 mg/mL BLG with 13 mM CdCl_2 , (b) 40 mg/mL BLG with 25 mM CdCl_2 , (c) 15 mg/mL BLG with 1.5 mM CdCl_2 , and (d) 40 mg/mL BLG with 3 mM CdCl_2 . All samples were prepared in D_2O .

In the following, we focus on the characterization of crystal growth within a MIP. Thus, samples in the region just below pseudo- c^{**} are selected as indicated by a yellow star in Figure 1.

Crystallization Followed by Optical Microscopy.

We now present the kinetics of nonclassical protein crystallization using optical microscopy. Samples containing 30 mg/mL BLG with 16, 17, and 18 mM CdCl_2 in D_2O (indicated by a yellow star in Figure 1) were prepared and followed by optical microscopy for several days. Directly after preparation, the solutions appear turbid due to the formation of aggregates developing a transient gel-like structure. The exact microscopic structure of the aggregates could not be resolved by optical microscopy due to the limited resolution. After roughly 1–2 h, the first crystals become visible and continue to grow for approximately 20 h. Simultaneously, the transient gel dissolves. Figure 3 shows representative snapshots of a sample containing

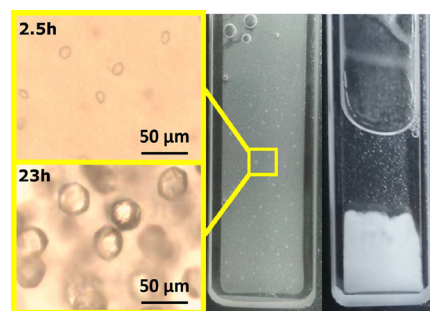


Figure 3. Nonclassical crystallization of BLG close to pseudo- c^{**} . A representative sample containing 30 mg/mL BLG and 17 mM CdCl_2 in D_2O at 21°C . In the early stage, a transient gel-like structure forms, which collapses due to consumption by crystal growth in the later stage, as can be seen in a quartz cuvette used for SANS experiments. Snapshots of the same sample are shown 2.5 and 23 h after preparation (left).

30 mg/mL BLG and 17 mM CdCl_2 after 2.5 and 23 h. Furthermore, it shows the transient gel formed directly after preparation and the sedimented crystals in the final state (after the transient gel has apparently been consumed by crystal growth) within the quartz cuvettes, which were used for SANS measurements.

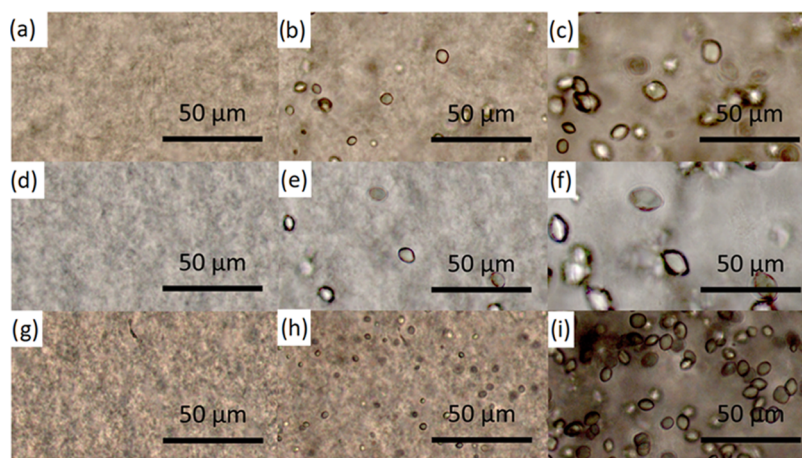


Figure 4. Optical microscopy images of 30 mg/mL BLG with CdCl₂: (a–c) 16 mM CdCl₂, (d–f) 17 mM CdCl₂, and (g–i) 18 mM CdCl₂ in D₂O different times after preparation. (a) Directly, (b) 9.5 h, and (c) 23 h after preparation; (d) directly, (e) 11 h, and (f) 3 days after preparation; (g) directly, (h) 7 h, and (i) 1 day after preparation.

In Figure 4, representative microscopy images of the real-time data of the crystallization process of 30 mg/mL BLG with 16, 17, and 18 mM CdCl₂ in D₂O are presented. As expected, the final crystal morphology is highly similar for all conditions studied in this region in the phase diagram (close to pseudo-*c*^{**}), i.e., roundish and compact (see Figures 2–4).

Crystal growth kinetics were determined from the real-time microscopy images by measuring the crystal side-to-side lengths at each time interval. Note that the isotropic shape implies that the crystal volume scales approximately with the cube of this length. The respective lengths are plotted in Figure 5 as a function of time. The linear portion of the data sets was

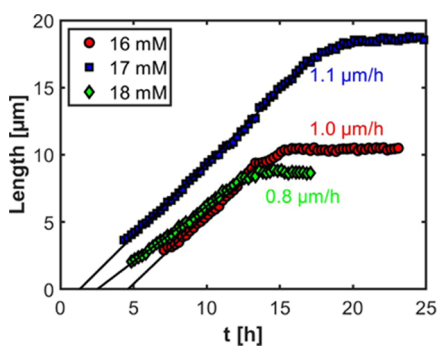


Figure 5. Crystal length as a function of time for 30 mg/mL BLG with 16, 17, and 18 mM CdCl₂ in D₂O.

fitted to obtain the growth rates and the induction times t_0 . For all samples, an initial linear growth followed by a saturation of the length can be observed. The crystals for the 17 mM sample grew the largest with a final size of roughly 20 μm and had the fastest induction time ($t_0 = 1.3$ h). The induction times for 16 and 18 mM were 4.6 and 2.5 h, respectively, indicating that nucleation occurred in all samples within 5 h. The respective growth rates are also shown in Figure 5. They denote that the samples containing 16 and 17 mM CdCl₂ grew approximately at the same speed, whereas the growth rate for the 18 mM sample was reduced. A clear trend as it can be observed for the system in H₂O that the crystal size increases with c_s is absent (see Figure S2). In comparison to H₂O, the induction time is longer, and the growth rate and the final crystal size are significantly reduced.

Crystallization Followed by Real-Time SANS. The same sample conditions (30 mg/mL BLG with 16, 17, and 18 mM CdCl₂ in D₂O) were studied by real-time SANS to obtain further kinetic information of the crystallization process. Since the neutron beam is much larger than an X-ray beam or the field of view in optical microscopy, we could ensure an excellent statistical average of the sample. Figure 6 shows the SANS intensities I as a function of scattering vector q and time t for each sample, respectively. Directly after preparation, the scattering intensity at very low q -values ($< 0.05 \text{ \AA}^{-1}$) is strongly increased due to the formation of amorphous aggregates. A broad correlation peak at $q \approx 0.175 \text{ \AA}^{-1}$ is visible, corresponding to a particle–particle distance of 36 \AA , which is the width of a BLG dimer.⁸⁰ An intermediate structural feature at $q \approx 0.075 \text{ \AA}^{-1}$ starts to develop from the beginning, corresponding to a particle–particle correlation distance of $d_{\text{MIP}} \approx 84 \text{ \AA}$. We identify this as the characteristic structural feature of the MIP, i.e., a local ordering of the proteins within the MIP. The MIP signal reaches a maximum in intensity after roughly 5 h and then decreases. Simultaneously to the decrease of MIP scattering, Bragg peaks appear at $q \approx 0.1, 0.12,$ and 0.2 \AA^{-1} and the intensity at very low q -values decreases again. The positions of the Bragg peaks are consistent with our previous SAXS measurements of the system in H₂O, suggesting a similar unit cell.²⁵

To identify possible correlations between the structural changes at different q -values and to clarify their role regarding crystallization, a two-phase analysis, originally known from the concept of crystallinity from semicrystalline polymer systems,⁸¹ was applied. In the first step, all curves $I(q, t)$ were normalized by the first curve $I(q, t = 0)$, which reveals the newly developing structures more clearly (see Figure 7a). In the second step, the overall background signal was considered by subtracting an appropriate linear background from the normalized data. The background was determined for each single curve separately by a linear fit through $I(q = 0.05 \text{ \AA}^{-1}, t)/I(q = 0.05 \text{ \AA}^{-1}, t = 0)$ and $I(q = 0.11 \text{ \AA}^{-1}, t)/I(q = 0.11 \text{ \AA}^{-1}, t = 0)$, respectively (indicated in Figure 7a by purple arrows). This interval enclosed by two local minima contains both the signal of the MIP and a Bragg peak and can therefore be used to determine the amount of the respective phases (MIP and crystals) within the samples at a given time. Since the q -region of the MIP overlaps with the first Bragg peak, we fitted the

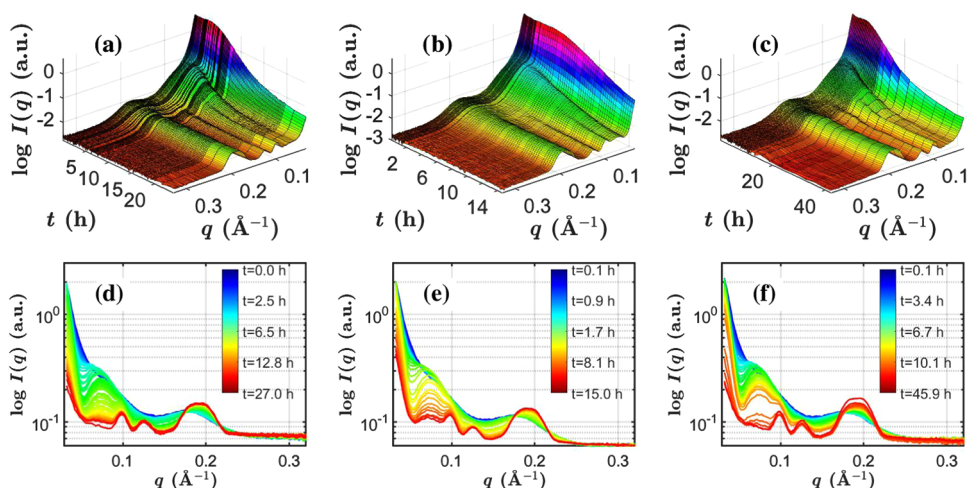


Figure 6. Nonclassical crystallization of BLG close to pseudo- c^{**} followed by real-time SANS: (a, d) 30 mg/mL BLG with 16 mM, (b, e) 17 mM, and (c, f) 18 mM CdCl_2 in D_2O at 20 °C. For each sample, SANS intensities $I(q, t)$ are plotted in two-dimensional (2D) and three-dimensional (3D) perspective. Note that the color code in 3D corresponds to the intensity, the color code in 2D illustrates the temporal evolution.

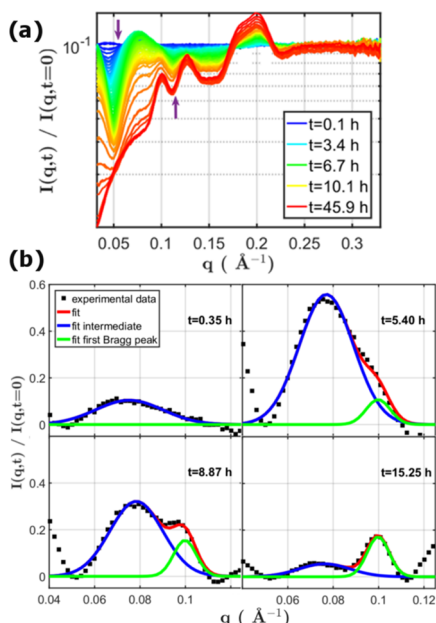


Figure 7. (a) Normalized SANS intensities $I(q, t)/I(q, t = 0)$ of 30 mg/mL BLG with 17 mM CdCl_2 . Normalization of the data reveals the newly developing structures more clearly. The interval for subsequent analysis is indicated by purple arrows. (b) Fits of background-corrected normalized SANS data in the low- q region: a sum of two Gaussians (red) with fixed center and width is used to separate the signal of the MIP (blue) and the first Bragg peak (green).

interval enclosed by a sum of two Gaussians, fixed in center and width. One Gaussian is fitted to the broad correlation peak apparently corresponding to the MIP and the second Gaussian is fitted to the first Bragg peak representing the crystals in the sample. To clarify this step of analysis, the normalized background-corrected data with fits at selected points of time are shown for 30 mg/mL BLG with 17 mM CdCl_2 in Figure 7b. Note that we did not perform any data analysis of particle shape or size employing form factors, but instead we focus on the distinct scattering features of correlation and Bragg peaks. Using this method, we can minimize the effect of sedimentation on the results, because sedimentation only causes an overall shift of the scattering curves toward higher

intensities due to the increase of the amount of material irradiated by the beam, which illuminates the bottom part of the cuvette. Since the analysis uses the area of well-defined peaks (correlation and Bragg peak) with an appropriate linear background correction, an overall upward shift of scattering profiles will not influence the analysis outcome. In addition, the illuminated area is big enough, and the medium viscosity is high enough that such sedimentation effects are minor.

Furthermore, the signal of the Bragg peak feature at $q \approx 0.2 \text{ \AA}^{-1}$ was evaluated in a model-free way. As a first step, a linear background through the intensity minima at $q_1 = 0.176 \text{ \AA}^{-1}$ and $q_2 = 0.217 \text{ \AA}^{-1}$ was subtracted from all normalized curves. In the second step, the normalized subtracted intensities were summed in the interval between the local minima for each time point. In the last step, the calculated sums were normalized by the maximum sum to obtain $A_{0.2 \text{ \AA}^{-1}}(t)$. The temporal evolution of the Bragg peak feature obtained by this method was similar to the ones presented (see Figure S1).

With the method discussed above, we derive a measure A of the signal of the MIP (A_{MIP}) and the first Bragg peak (A_{Bragg}) by calculating the area under the respective Gaussian functions as a function of time. $A(t)$ thus provides information on crystal growth and the evolution of the MIP. Subsequently, we calculated the first time derivative of the Bragg peak signal $(d/dt)A_{\text{Bragg}}$ from the green guide to the eye in Figure 8 to compare the crystal growth rate with the evolution of the MIP. The results are presented in Figure 8 for 16, 17, and 18 mM CdCl_2 .

In Figure 8, one can see that the MIP starts to form directly after preparation, and 1–2 h later, the Bragg peaks start to grow, indicating the formation of crystals. The MIP passes a maximum after roughly 5 h and levels off again within the next 20 h. Simultaneously, crystal growth saturates. Both saturations are a clear sign against sedimentation of material into the beam. The analysis reveals that the crystal growth rates are at their respective maxima when a large amount of the MIP is available. It also reveals that the maximum of A_{MIP} is slightly delayed (≈ 1 –2 h) with respect to the maximum of $(d/dt)A_{\text{Bragg}}$, suggesting that crystals already start to form as soon as some amount of MIP is developed. We note that for the sample with the longest measurement time, we observed a second growth stage of the Bragg signal after 35 h, being

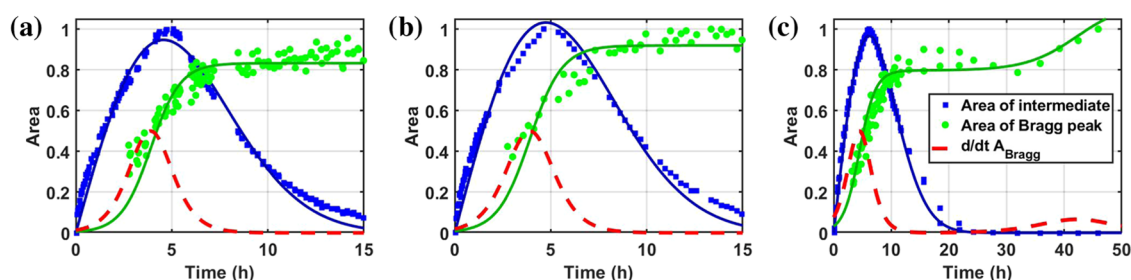


Figure 8. Normalized kinetic analysis of 30 mg/mL BLG close to pseudo- c^* : correlations between the evolution of the MIP and the Bragg peaks for 30 mg BLG with (a) 16 mM CdCl_2 , (b) 17 mM CdCl_2 , and (c) 18 mM CdCl_2 . The MIP starts to grow directly after preparation and passes a maximum. Bragg peaks start to grow slightly later. At the same time, as the amount of MIP decreases again, the growth of the Bragg peaks reaches saturation. A second growth stage of the Bragg peaks is observed after roughly 35 h. The colored lines are a guide to the eye.

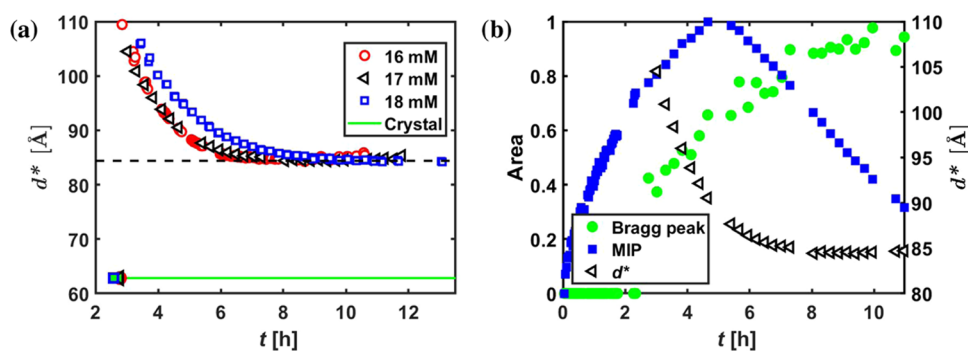


Figure 9. (a) Average distance between two proteins d^* within the MIP as a function of time for samples containing 30 mg/mL BLG and 16, 17, and 18 mM CdCl_2 . In green, the crystal distance corresponding to the first Bragg peak at 0.1 \AA^{-1} is shown with the respective symbols indicating when the Bragg peak was observed by SANS (see Figure 8). The black dashed line at $d = 84 \text{ \AA}$ indicates a similar final distance within the MIP for all three c_s . (b) Amount of MIP (filled blue squares) and crystalline phase (filled green circles) as well as d^* (open black triangles) as a function of time for a sample containing 30 mg/mL BLG and 17 mM CdCl_2 . Filled symbols correspond to the left y-axis, whereas open symbols correspond to the right y-axis.

consistent with our previous studies in H_2O using SAXS.^{25,26} However, similar to the data in H_2O , no second growth step can be seen in the microscopy data either (see Figures 5 and S3).

We note that the rate of crystallization strongly depends on the respective batch of protein since BLG has a purity of only 90%. While the general phase behavior (RC) is observed for every batch, the phase transition boundaries and the crystallization speed vary. Investigating a similar condition (33 mg/mL BLG and 17 mM CdCl_2 in D_2O), measured with a different batch of protein on a different beamtime, resulted in a fast crystallization that was completed within 2 h (see Figure S2). In this case, the data analysis shows also a clear two-step crystal growth. In combination with Figure 8 and the previous studies in H_2O ,^{25,26} we conclude that the second growth stage is a relevant feature and is caused by crystal growth within the dilute phase after all MIP is consumed and not only by crystals sedimenting into the beam. It is worth noting that the second growth stage (of the SANS signal) may only improve the crystal quality but not its size,⁸² which would explain the absence of this growth stage in the microscopy data.

Finally, we analyze the structure of the MIP as a function of time. For this purpose, a Gaussian was fitted to the MIP correlation peak of the SANS data shown in Figure 6. The q -values of the respective maxima (q^*) were transformed into real space distances by $d^* = 2\pi/q^*$. These values are plotted in Figure 9a. It is clearly visible that the proteins within the MIP are initially correlated within a range of 105–110 Å. With time, the average distance between the particles in the MIP

decreases to 84 Å, where it saturates for all c_s investigated. Note that d^* is the average distance, but the correlation peak has a certain width, hence, shorter and longer distances are also present within the MIP and fully evolved domains may already serve as crystal precursors. Similarly, in a Lennard-Jones system at moderate supercooling, a local order parameter distribution was found.³⁷ Since d^* changes with time, the MIP is assumed to be protein aggregates with a certain flexibility. To compare the development of the MIP with the overall amount of MIP and crystals, all three parameters are plotted for 30 mg/mL BLG with 17 mM CdCl_2 in Figure 9b. Here, the maximum amount of dense phase present in the sample is close to the saturation time of d^* . Hence, when the maximum amount of MIP is present, the average distance between the proteins is at its final stage and a maximum amount of preordered precursor is available for crystallization. Roughly at this time, the crystallization rate is the highest, indicating the important role of a fully developed MIP as a preordered precursor. Based on the SANS analysis, we expect the MIP to be locally preordered domains. Hence, we conclude that in our system, first, the order changes within the clusters (see Figure 9) and subsequently the density. However, the MIP does not necessarily already have the similar structure as the final crystal.

DISCUSSION ON THE ROLE AND THE DEVELOPMENT OF THE MIP

We discuss the significance of the preordered MIP observed in this work in comparison with other protein systems. In the BLG- CdCl_2 system, gel-like aggregates are formed in the

condensed regime II instead of LLPS.^{25,26} The metastable aggregates develop a correlation peak at $q \approx 0.075 \text{ \AA}^{-1}$ in SANS and SAXS measurements, which is close to the first Bragg peak at $q = 0.1 \text{ \AA}^{-1}$, indicating the preordered nature of this MIP. In our previous work on the system HSA with CeCl_3 , a metastable LLPS with respect to crystallization was found.⁶² Thus, dense liquid droplets were identified as metastable intermediates between solution and crystals.⁶² However, these droplets seem to act only as a reservoir rather than precursors and no structural feature such as a correlation peak was observed in SAXS/SANS data.⁶² In BLG with ZnCl_2 solutions,^{24,24} amorphous aggregates form initially in regime II, but they relax into a dense liquid state. Crystals appear at the interface of the dense phase and grow into the surrounding dilute phase.²⁴ Neither the initial amorphous aggregates nor the dense liquid phase show such a correlation peak in scattering profiles. Interestingly, for BLG with YCl_3 ,⁸³ a correlation peak was observed at $q \approx 0.03 \text{ \AA}^{-1}$ in comparison with the first Bragg peak at $q = 0.92 \text{ \AA}^{-1}$.⁸⁴ This correlation peak was attributed to a local order of protein clusters caused by the fine balance between the bridging effect of metal ions and the electrostatic repulsion due to the accumulated net charges close to c^{**} .⁸³ Hence, it seems that the correlation peak observed here (and in H_2O ^{24,25}) is indeed a sign of preordering within the MIP, which cannot be seen for conditions close to c^* , which are believed to follow a one-step crystallization pathway.^{24,25}

Similar preordering has been reported for ferritin crystallization in the presence of Cd^{2+} .⁵² There, the preordered protein aggregates have an interparticle distance of less than 1.3 times the distance in the crystal and the crystalline order evolution is accompanied with the shortening of the interparticle distance.⁵² This phenomenon has been observed also in mineralization processes and dehydration is proposed to be the driver of this change of distance.^{35,48,52} In our system, the first Bragg peak corresponds to an interparticle distance of 62 Å and if we multiply it by 1.3, the nearest neighbors should be within a distance of roughly 80 Å. If water is expelled from the crystal during the final stage,³⁵ but is still present within the preordered MIP, the determined saturation interparticle distance of $d = 84 \text{ \AA}$ within the MIP can be interpreted as the distance of nearest neighbors. Since d^* decreases from initially $\approx 110 \text{ \AA}$ to the final value of $d_{\text{MIP}} = 84 \text{ \AA}$, the number of nearest neighbors increases in this process as well, or, in other words, a densification occurs parallel to the structural changes. Based on these discussions, the crystallization pathway revealed in this work is illustrated in Figure 10.

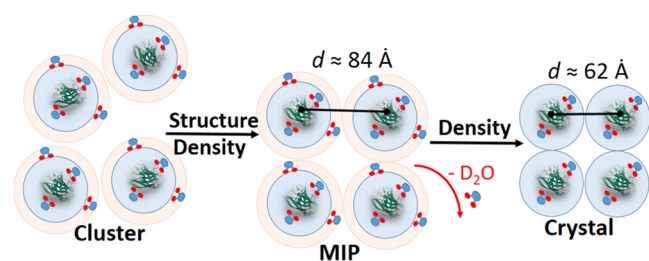


Figure 10. Schematic pathway of protein crystallization from a metastable intermediate phase revealed in this work. The BLG monomers are drawn in green (PDB entry 4LZU, visualized by Mol*⁹²). The oxygen atoms of D_2O are colored blue, whereas the deuterium atoms are colored red. For clarity, Cd^{2+} ions are not drawn.

Directly after preparation, randomly oriented clusters form. They undergo a preordering and a first densification in parallel, until an interparticle distance of $d = 84 \text{ \AA}$ within the MIP is reached. As a second step, D_2O is expelled and therefore the density increases again, resulting in the final crystal with an interparticle distance of $d = 62 \text{ \AA}$. This $\approx 20 \text{ \AA}$ difference between MIP and crystal is believed to correspond to the release of roughly two layers of water from each protein involved, since the first hydration layer of a protein was found to be 3–5 Å thick while the overall hydration layer can be up to 8 Å.^{85–88} We note that in this study heavy water (D_2O) and not H_2O was used as a solvent, which might influence the hydration slightly.

Another feature of the MIP is the mobility of molecules within the aggregates. Since the solutions investigated are extremely viscous and gel-like after preparation (see Figure 3), a certain degree of mobility of molecules is assumed to be needed for crystallization. In an extreme case of glass, it was found that the rigidity of the network plays a crucial role in phase transitions (and therefore nucleation).⁸⁹ Nucleation is believed to occur in so-called “active centers”, namely, the dynamic regions of the network, which are able to spatially rearrange and move within the rigid network.⁸⁹ Below a certain threshold, the sizes of these dynamic regions are too small for nucleation.⁸⁹ Ordering occurs first in these dynamic regions, followed by an increasing density (lowering of entropy).^{89,90} A recent study on protein crystallization using time-resolved liquid-cell TEM demonstrated that proteins in the lattice are mobile throughout the crystal structure in the early stage of crystallization.⁹¹ The intermolecular bonds or contacts can break and reform rapidly,⁹¹ supporting the hypothesis of flexible and dynamic intermediates. Our previous work on the crystallization of BLG in the presence of YCl_3 showed that the protein clusters have not only a precrystalline structure but also an internal flexibility, which enables local reorientation within the clusters.⁸⁴ In consistency with this work, the temporal evolution of the ordering indicates that, although a local order exists, proteins are supposed to be still flexible within the MIP and can rearrange themselves, which is crucial for these aggregates being nucleation precursors.

CONCLUSIONS

In summary, we demonstrate that the combination of real-time SANS and optical microscopy can be used to reveal new insights into the kinetics of protein crystallization. Based on our findings, we suggest the following nonclassical crystallization mechanism: directly after preparation, the proteins form big amorphous aggregates. Within these aggregates, a preordered structure starts to develop (MIP) on a length scale slightly larger than the crystal unit cell. Since preordering lowers the nucleation barrier of the protein molecules, crystals start to nucleate within the MIP. Potentially, D_2O is expelled in the final stage as closing densification. During nucleation, the MIP is consumed. The crystals may grow further upon consuming a fraction of the proteins of the solution until a final equilibrium between solution and crystals is reached. These findings of a preordered precursor pave the way for understanding the crystallization pathway and the temporal role of a MIP during crystallization in aqueous protein solutions. This is not only relevant from a fundamental point of view but also has a huge impact on structural biology and potentially many other fields like biopharmaceutical formulation.

■ ASSOCIATED CONTENT

SI Supporting Information

The Supporting Information is available free of charge at <https://pubs.acs.org/doi/10.1021/acs.cgd.1c00908>.

Further SANS data and analysis and optical microscopy analysis (PDF)

■ AUTHOR INFORMATION

Corresponding Author

Fajun Zhang – Institut für Angewandte Physik, Universität Tübingen, 72076 Tübingen, Germany; orcid.org/0000-0001-7639-8594; Email: fajun.zhang@uni-tuebingen.de

Authors

Ralph Maier – Institut für Angewandte Physik, Universität Tübingen, 72076 Tübingen, Germany; orcid.org/0000-0003-3428-039X

Benedikt Sohmen – Institut für Angewandte Physik, Universität Tübingen, 72076 Tübingen, Germany

Stefano Da Vela – Institut für Angewandte Physik, Universität Tübingen, 72076 Tübingen, Germany; Present Address: EMBL c/o DESY, Notkestr. 85, Geb. 25a, 22607 Hamburg, Germany

Olga Matsarskaia – Institut für Angewandte Physik, Universität Tübingen, 72076 Tübingen, Germany; Present Address: Institut Laue - Langevin, 71 Avenue des Martyrs, CS 20 156, 38042 Grenoble CEDEX 9, France; orcid.org/0000-0002-7293-7287

Christian Beck – Institut Laue—Langevin, 38042 Grenoble, France; orcid.org/0000-0001-7214-3447

Ralf Schweins – Institut Laue—Langevin, 38042 Grenoble, France

Tilo Seydel – Institut Laue—Langevin, 38042 Grenoble, France; orcid.org/0000-0001-9630-1630

Frank Schreiber – Institut für Angewandte Physik, Universität Tübingen, 72076 Tübingen, Germany; orcid.org/0000-0003-3659-6718

Complete contact information is available at: <https://pubs.acs.org/doi/10.1021/acs.cgd.1c00908>

Notes

The authors declare no competing financial interest.

■ ACKNOWLEDGMENTS

The authors gratefully acknowledge the financial support from the DFG and the allocation of beamtime (doi: 10.5291/ILL-DATA.9-13-620 and doi: 10.5291/ILL-DATA.9-13-672) at D11, ILL, Grenoble, France. They also thank Aafiya Idrees and Marcus Mikorski for experimental assistance. F.Z. expresses thanks for the support from the Open Research Fund of the State Key Laboratory of Polymer Physics and Chemistry, Changchun Institute of Applied Chemistry, Chinese Academy of Sciences.

■ REFERENCES

- (1) Puhl, S.; Meinel, L.; Germershaus, O. Recent advances in crystalline and amorphous particulate protein formulations for controlled delivery. *Asian J. Pharm. Sci.* **2016**, *11*, 469–477.
- (2) Vaishya, R.; Khurana, V.; Patel, S.; Mitra, A. K. Long-term delivery of protein therapeutics. *Expert Opin. Drug Delivery* **2015**, *12*, 415–440.

- (3) Durbin, S. D.; Feher, G. Protein crystallization. *Annu. Rev. Phys. Chem.* **1996**, *47*, 171–204.
- (4) Volmer, M.; Weber, A. Germ-formation in oversaturated figures. *Z. Phys. Chem.* **1926**, *119*, 277–301.
- (5) Kashchiev, D. *Nucleation*; Butterworth-Heinemann, 2000.
- (6) Gebauer, D.; Cölfen, H. Prenucleation clusters and non-classical nucleation. *Nano Today* **2011**, *6*, 564–584.
- (7) Anderson, V. J.; Lekkerkerker, H. N. W. Insights into phase transition kinetics from colloid science. *Nature* **2002**, *416*, 811–815.
- (8) Sear, R. Nucleation at contact lines where fluid-fluid interfaces meet solid surfaces. *J. Phys.: Condens. Matter* **2007**, *19*, No. 466106.
- (9) ten Wolde, P. R.; Frenkel, D. Enhancement of Protein Crystal Nucleation by Critical Density Fluctuations. *Science* **1997**, *277*, 1975–1978.
- (10) Vekilov, P. G. Dense Liquid Precursor for the Nucleation of Ordered Solid Phases from Solution. *Cryst. Growth Des.* **2004**, *4*, 671–685.
- (11) Wallace, A. F.; Hedges, L. O.; Fernandez-Martinez, A.; Raiteri, P.; Gale, J. D.; Waychunas, G. A.; Whitlam, S.; Banfield, J. F.; De Yoreo, J. J. Microscopic Evidence for Liquid-Liquid Separation in Supersaturated CaCO₃ Solutions. *Science* **2013**, *341*, 885–889.
- (12) Sear, R. P. The non-classical nucleation of crystals: microscopic mechanisms and applications to molecular crystals, ice and calcium carbonate. *Int. Mater. Rev.* **2012**, *57*, 328–356.
- (13) Maes, D.; Vorontsova, M. A.; Potenza, M. A. C.; Sanvito, T.; Sleutel, M.; Giglio, M.; Vekilov, P. G. Do protein crystals nucleate within dense liquid clusters? *Acta Crystallogr., Sect. F: Struct. Biol. Commun.* **2015**, *71*, 815–822.
- (14) Harland, J. L.; Henderson, S. I.; Underwood, S. M.; van Megen, W. Observation of Accelerated Nucleation in Dense Colloidal Fluids of Hard Sphere Particles. *Phys. Rev. Lett.* **1995**, *75*, 3572–3575.
- (15) Martin, S.; Bryant, G.; van Megen, W. Crystallization kinetics of polydisperse colloidal hard spheres: Experimental evidence for local fractionation. *Phys. Rev. E* **2003**, *67*, No. 061405.
- (16) Martin, S.; Bryant, G.; van Megen, W. Crystallization kinetics of polydisperse colloidal hard spheres. II. Binary mixtures. *Phys. Rev. E* **2005**, *71*, No. 021404.
- (17) Schöpe, H. J.; Bryant, G.; van Megen, W. Two-Step Crystallization Kinetics in Colloidal Hard-Sphere Systems. *Phys. Rev. Lett.* **2006**, *96*, No. 175701.
- (18) Schilling, T.; Schöpe, H. J.; Oettel, M.; Opletal, G.; Snook, I. Precursor-Mediated Crystallization Process in Suspensions of Hard Spheres. *Phys. Rev. Lett.* **2010**, *105*, No. 025701.
- (19) Galkin, O.; Vekilov, P. G. Control of protein crystal nucleation around the metastable liquid-liquid phase boundary. *Proc. Natl. Acad. Sci. U.S.A.* **2000**, *97*, 6277–6281.
- (20) Galkin, O.; Vekilov, P. G. Are Nucleation Kinetics of Protein Crystals Similar to Those of Liquid Droplets. *J. Am. Chem. Soc.* **2000**, *122*, 156–163.
- (21) Chen, Q.; Vekilov, P. G.; Nagel, R. L.; Hirsch, R. E. Liquid-Liquid Phase Separation in Hemoglobins: Distinct Aggregation Mechanisms of the $\beta 6$ Mutants. *Biophys. J.* **2004**, *86*, 1702–1712.
- (22) Gebauer, D.; Völkel, A.; Cölfen, H. Stable prenucleation calcium carbonate clusters. *Science* **2008**, *322*, 1819–1822.
- (23) Vekilov, P. G. Nucleation. *Cryst. Growth Des.* **2010**, *10*, S007–S019.
- (24) Sauter, A.; Oelker, M.; Zocher, G.; Zhang, F.; Stehle, T.; Schreiber, F. Nonclassical Pathways of Protein Crystallization in the Presence of Multivalent Metal Ions. *Cryst. Growth Des.* **2014**, *14*, 6357–6366.
- (25) Sauter, A.; Roosen-Runge, F.; Zhang, F.; Lotze, G.; Jacobs, R. M. J.; Schreiber, F. Real-Time Observation of Nonclassical Protein Crystallization Kinetics. *J. Am. Chem. Soc.* **2015**, *137*, 1485–1491.
- (26) Sauter, A.; Roosen-Runge, F.; Zhang, F.; Lotze, G.; Feoktystov, A.; Jacobs, R. M. J.; Schreiber, F. On the question of two-step nucleation in protein crystallization. *Faraday Discuss.* **2015**, *179*, 41–58.

- (27) Sleutel, M.; van Driessche, A. E. S. Role of clusters in nonclassical nucleation and growth of protein crystals. *Proc. Nat. Sci. U.S.A.* **2014**, *111*, E546–E553.
- (28) Sleutel, M.; Lutsko, J. F.; Maes, D.; Van Driessche, A. E. S. Mesoscopic Impurities Expose a Nucleation-Limited Regime of Crystal Growth. *Phys. Rev. Lett.* **2015**, *114*, No. 245501.
- (29) Gebauer, D.; Wolf, S. E. Designing solid materials from their solute state: a shift in paradigms toward a holistic approach in functional materials chemistry. *J. Am. Chem. Soc.* **2019**, *141*, 4490–4504.
- (30) Gebauer, D.; Kellermeier, M.; Gale, J. D.; Bergström, L.; Cölfen, H. Pre-nucleation clusters as solute precursors in crystallization. *Chem. Soc. Rev.* **2014**, *43*, 2348–2371.
- (31) Zhang, F. Nonclassical nucleation pathways in protein crystallization. *J. Phys.: Condens. Matter* **2017**, *29*, No. 443002.
- (32) Karthika, S.; Radhakrishnan, T.; Kalaichelvi, P. A review of classical and nonclassical nucleation theories. *Cryst. Growth Des.* **2016**, *16*, 6663–6681.
- (33) Zhang, T. H.; Liu, X. Y. How does a transient amorphous precursor template crystallization. *J. Am. Chem. Soc.* **2007**, *129*, 1320–13526.
- (34) Soga, K. G.; Melrose, J. R.; Ball, R. C. Metastable States and the Kinetics of Colloid Phase Separation. *J. Chem. Phys.* **1999**, *110*, 2280–2289.
- (35) Sebastiani, F.; Wolf, S. L.; Born, B.; Luong, T. Q.; Cölfen, H.; Gebauer, D.; Havenith, M. Water dynamics from THz spectroscopy reveal the locus of a liquid-liquid binodal limit in aqueous CaCO₃ solutions. *Angew. Chem., Int. Ed.* **2017**, *56*, 490–495.
- (36) Zhang, F.; Gavira, J. A.; Lee, G. W.; Zahn, D. Nonclassical Nucleation—Role of Metastable Intermediate Phase in Crystal Nucleation: An Editorial Prefix. *Crystals* **2021**, *11*, No. 174.
- (37) Ten Wolde, P. R.; Ruiz-Montero, M. J.; Frenkel, D. Numerical evidence for bcc ordering at the surface of a critical fcc nucleus. *Phys. Rev. Lett.* **1995**, *75*, No. 2714.
- (38) Chung, S.-Y.; Kim, Y.-M.; Kim, J.-G.; Kim, Y.-J. Multiphase transformation and Ostwald's rule of stages during crystallization of a metal phosphate. *Nat. Phys.* **2009**, *5*, 68–73.
- (39) Ranguelov, B.; Nanev, C. 2D Monte Carlo simulation of patchy particles association and protein crystal polymorph selection. *Crystals* **2019**, *9*, No. 508.
- (40) Park, B. C.; Cho, J.; Kim, M. S.; Ko, M. J.; Pan, L.; Na, J. Y.; Kim, Y. K. Strategy to control magnetic coercivity by elucidating crystallization pathway-dependent microstructural evolution of magnetite mesocrystals. *Nat. Commun.* **2020**, *11*, No. 298.
- (41) Kezuka, Y.; Kawai, K.; Eguchi, K.; Tajika, M. Fabrication of single-crystalline calcite needle-like particles using the aragonite-calcite phase transition. *Minerals* **2017**, *7*, No. 133.
- (42) Mirabello, G.; Ianiro, A.; Bomans, P. H.; Yoda, T.; Arakaki, A.; Friedrich, H.; de With, G.; Sommerdijk, N. A. Crystallization by particle attachment is a colloidal assembly process. *Nat. Mater.* **2020**, *19*, 391–396.
- (43) Tidhar, Y.; Weissman, H.; Tworowski, D.; Rybtchinski, B. Mechanism of crystalline self-assembly in aqueous medium: a combined cryo-TEM/kinetic study. *Chem. - Eur. J.* **2014**, *20*, 10332–10342.
- (44) De Yoreo, J. J.; Gilbert, P. U. P. A.; Sommerdijk, N. A. J. M.; Penn, R. L.; Whitelam, S.; Joester, D.; Zhang, H.; Rimer, J. D.; Navrotsky, A.; Banfield, J. F.; Wallace, A. F.; Michel, F. M.; Meldrum, F. C.; Cölfen, H.; Dove, P. M. Crystallization by particle attachment in synthetic, biogenic, and geologic environments. *Science* **2015**, *349*, No. aaa6760.
- (45) Wu, H.; Yang, Y.; Ou, Y.; Lu, B.; Li, J.; Yuan, W.; Wang, Y.; Zhang, Z. Early stage growth of rutile titania mesocrystals. *Cryst. Growth Des.* **2018**, *18*, 4209–4214.
- (46) Jehannin, M.; Rao, A.; Cölfen, H. New horizons of nonclassical crystallization. *J. Am. Chem. Soc.* **2019**, *141*, 10120–10136.
- (47) Van Driessche, A. E.; Van Gerven, N.; Bomans, P. H.; Joosten, R. R.; Friedrich, H.; Gil-Carton, D.; Sommerdijk, N. A.; Sleutel, M. Molecular nucleation mechanisms and control strategies for crystal polymorph selection. *Nature* **2018**, *556*, 89–94.
- (48) Lam, R. S.; Charnock, J. M.; Lennie, A.; Meldrum, F. C. Synthesis-dependant structural variations in amorphous calcium carbonate. *CrystEngComm* **2007**, *9*, 1226–1236.
- (49) Wiedenbeck, E.; Kovermann, M.; Gebauer, D.; Cölfen, H. Liquid Metastable Precursors of Ibuprofen as Aqueous Nucleation Intermediates. *Angew. Chem., Int. Ed.* **2019**, *58*, 19103–19109.
- (50) Lu, Y.; Lu, X.; Qin, Z.; Shen, J. Experimental evidence for ordered precursor foreshadowing crystal nucleation in colloidal system. *Solid State Commun.* **2015**, *217*, 13–16.
- (51) Tsarafati, Y.; Rosenne, S.; Weissman, H.; Shimon, L. J.; Gur, D.; Palmer, B. A.; Rybtchinski, B. Crystallization of organic molecules: Nonclassical mechanism revealed by direct imaging. *ACS Cent. Sci.* **2018**, *4*, 1031–1036.
- (52) Houben, L.; Weissman, H.; Wolf, S. G.; Rybtchinski, B. A mechanism of ferritin crystallization revealed by cryo-STEM tomography. *Nature* **2020**, *579*, 540–543.
- (53) Sleutel, M.; Lutsko, J.; van Driessche, A. E.; Durán-Olivencia, M. A.; Maes, D. Observing classical nucleation theory at work by monitoring phase transitions with molecular precision. *Nat. Commun.* **2014**, *5*, No. 5598.
- (54) Zhang, F.; Skoda, M. W. A.; Jacobs, R. M. J.; Zorn, S.; Martin, R. A.; Martin, C. M.; Clark, G. F.; Weggler, S.; Hildebrandt, A.; Kohlbacher, O.; Schreiber, F. Reentrant Condensation of Proteins in Solution Induced by Multivalent Counterions. *Phys. Rev. Lett.* **2008**, *101*, No. 148101.
- (55) Zhang, F.; Weggler, S.; Ziller, M. J.; Ianeselli, L.; Heck, B. S.; Hildebrandt, A.; Kohlbacher, O.; Skoda, M. W. A.; Jacobs, R. M. J.; Schreiber, F. Universality of protein reentrant condensation in solution induced by multivalent metal ions. *Proteins* **2010**, *78*, 3450–3457.
- (56) Roosen-Runge, F.; Heck, B. S.; Zhang, F.; Kohlbacher, O.; Schreiber, F. Interplay of pH and Binding of Multivalent Metal Ions: Charge Inversion and Reentrant Condensation in Protein Solutions. *J. Phys. Chem. B* **2013**, *117*, 5777–5787.
- (57) Zhang, F.; Roosen-Runge, F.; Sauter, A.; Wolf, M.; Jacobs, R. M. J.; Schreiber, F. Reentrant Condensation, Liquid-Liquid Phase Separation and Crystallization in Protein Solutions Induced by Multivalent Metal Ions. *Pure Appl. Chem.* **2014**, *86*, 191–202.
- (58) Soraruf, D.; Roosen-Runge, F.; Grimaldo, M.; Zanini, F.; Schweins, R.; Seydel, T.; Zhang, F.; Roth, R.; Oettel, M.; Schreiber, F. Protein cluster formation in aqueous solution in the presence of multivalent metal ions - a light scattering study. *Soft Matter* **2014**, *10*, 894–902.
- (59) Zhang, F.; Zocher, G.; Sauter, A.; Stehle, T.; Schreiber, F. Novel approach to controlled protein crystallization through ligandation of yttrium cations. *J. Appl. Crystallogr.* **2011**, *44*, 755–762.
- (60) Roosen-Runge, F.; Zhang, F.; Schreiber, F.; Roth, R. Ion-activated Attractive Patches as a Mechanism for Controlled Protein Interactions. *Sci. Rep.* **2015**, *4*, No. 7016.
- (61) Wolf, M.; Roosen-Runge, F.; Zhang, F.; Roth, R.; Skoda, M. W.; Jacobs, R. M.; Sztucki, M.; Schreiber, F. Effective interactions in protein-salt solutions approaching liquid-liquid phase separation. *J. Mol. Liq.* **2014**, *200*, 20–27.
- (62) Maier, R.; Zocher, G.; Sauter, A.; Da Vela, S.; Matsarskaia, O.; Schweins, R.; Sztucki, M.; Zhang, F.; Stehle, T.; Schreiber, F. Protein Crystallization in the Presence of a Metastable Liquid-Liquid Phase Separation. *Cryst. Growth Des.* **2020**, *20*, 7951–7962.
- (63) Matsarskaia, O.; Roosen-Runge, F.; Schreiber, F. Multivalent ions and biomolecules: Attempting a comprehensive perspective. *ChemPhysChem* **2020**, *21*, 1742–1767.
- (64) Haas, C.; Drenth, J. Understanding protein crystallization on the basis of the phase diagram. *J. Cryst. Growth* **1999**, *196*, 388–394.
- (65) Beck, C.; Grimaldo, M.; Roosen-Runge, F.; Maier, R.; Matsarskaia, O.; Braun, M.; Sohmen, B.; Czakkel, O.; Schweins, R.; Zhang, F.; Seydel, T.; Schreiber, F. Following Protein Dynamics in Real Time during Crystallization. *Cryst. Growth Des.* **2019**, *19*, 7036–7045.

- (66) Ou, Z.; Wang, Z.; Luo, B.; Luijten, E.; Chen, Q. Kinetic pathways of crystallization at the nanoscale. *Nat. Mater.* **2020**, *19*, 450–455.
- (67) Schubert, R.; Meyer, A.; Baitan, D.; Dierks, K.; Perbandt, M.; Betzel, C. Real-Time Observation of Protein Dense Liquid Cluster Evolution during Nucleation in Protein Crystallization. *Cryst. Growth Des.* **2017**, *17*, 954–958.
- (68) Sober, H. A. *CRC Handbook of Biochemistry: Selected Data for Molecular Biology*; The Chemical Rubber Co.: Cleveland, Ohio, 1970.
- (69) Krężel, A.; Bał, W. A formula for correlating pKa values determined in D₂O and H₂O. *J. Inorg. Biochem.* **2004**, *98*, 161–166.
- (70) Covington, A. K.; Paabo, M.; Robinson, R. A.; Bates, R. G. Use of the glass electrode in deuterium oxide and the relation between the standardized pD (paD) scale and the operational pH in heavy water. *Anal. Chem.* **1968**, *40*, 700–706.
- (71) Elofsson, U. M.; Paulsson, M. A.; Arnebrant, T. Adsorption of β -Lactoglobulin A and B in Relation to Self-Association: Effect of Concentration and pH. *Langmuir* **1997**, *13*, 1695–1700.
- (72) Lieutenant, K.; Lindner, P.; Gähler, R. A new design for the standard pinhole small-angle neutron scattering instrument D11. *J. Appl. Crystallogr.* **2007**, *40*, 1056–1063.
- (73) Könnicke, M.; Akeroyd, F. A.; Bernstein, H. J.; Brewster, A. S.; Campbell, S. I.; Clausen, B.; Cottrell, S.; Hoffmann, J. U.; Jemian, P. R.; Männicke, D.; et al. The NeXus data format. *J. Appl. Crystallogr.* **2015**, *48*, 301–305.
- (74) Richard, D.; Ferrand, M.; J Kearley, G. Analysis and visualisation of neutron-scattering data. *J. Neutron Res.* **1996**, *4*, 33–39.
- (75) Zhang, F.; Beck, C.; Feustel, M.; Da Vela, S.; Maier, R.; Matsarskaia, O.; Mikorski, M.; Roosen-Runge, F.; Schreiber, F.; Schweins, R.; Seydel, T.; Sohmen, B. Kinetics of Two-Step Nucleation in Protein Crystallization Studied by Real-Time SANS; Institut Laue-Langevin (ILL), 2016. <http://dx.doi.org/10.5291/ILL-DATA.9-13-672>.
- (76) Zhang, F.; Da Vela, S.; Feustel, M.; Grimaldo, M.; Matsarskaia, O.; Roosen-Runge, F.; Schreiber, F.; Schweins, R.; Seydel, T.; Sohmen, B. Kinetics of Two-Step Nucleation in Protein Crystallization Studied by Real-Time SANS; Institut Laue-Langevin (ILL), 2015. <http://dx.doi.org/10.5291/ILL-DATA.9-13-620>.
- (77) Braun, M. K.; Wolf, M.; Matsarskaia, O.; Da Vela, S.; Roosen-Runge, F.; Sztucki, M.; Roth, R.; Zhang, F.; Schreiber, F. Strong Isotope Effects on Effective Interactions and Phase Behavior in Protein Solutions in the Presence of Multivalent Ions. *J. Phys. Chem. B* **2017**, *121*, 1731–1739.
- (78) Trakhanov, S.; Quiocho, F. A. Influence of divalent cations in protein crystallization. *Protein Sci.* **1995**, *4*, 1914–1919.
- (79) Trakhanov, S.; Kreimer, D. I.; Parkin, S.; Ames, G. F.-L.; Rupp, B. Cadmium-induced crystallization of proteins: II. Crystallization of the salmonella typhimurium histidine-binding protein in complex with L-histidine, L-arginine, or L-lysine. *Protein Sci.* **1998**, *7*, 600–604.
- (80) Verheul, M.; Pedersen, J. S.; Roefs, S. P. F. M.; de Kruif, K. G. Association Behavior of Native β -Lactoglobulin. *Biopolymers* **1999**, *49*, 11–20.
- (81) Strobl, G. *The Physics of Polymers*, 3rd ed.; Springer: Berlin, Heidelberg, 2007; Chapter 5.
- (82) Flood, A. E. Feedback between crystal growth rates and surface roughness. *CrystEngComm* **2010**, *12*, 313–323.
- (83) Sauter, A.; Zhang, F.; Szekely, N. K.; Pipich, V.; Sztucki, M.; Schreiber, F. Structural Evolution of Metastable Protein Aggregates in the Presence of Trivalent Salt Studied by (V)SANS and SAXS. *J. Phys. Chem. B* **2016**, *120*, 5564–5571.
- (84) Zhang, F.; Roosen-Runge, F.; Sauter, A.; Roth, R.; Skoda, M. W. A.; Jacobs, R.; Sztucki, M.; Schreiber, F. The Role of Cluster Formation and Metastable Liquid-Liquid Phase Separation in Protein Crystallization. *Faraday Discuss.* **2012**, *159*, 313–325.
- (85) Sinha, S. K.; Chakraborty, S.; Bandyopadhyay, S. Thickness of the hydration layer of a protein from molecular dynamics simulation. *J. Phys. Chem. B* **2008**, *112*, 8203–8209.
- (86) Bandyopadhyay, S.; Chakraborty, S.; Balasubramanian, S.; Pal, S.; Bagchi, B. Atomistic simulation study of the coupled motion of amino acid residues and water molecules around protein HP-36: fluctuations at and around the active sites. *J. Phys. Chem. B* **2004**, *108*, 12608–12616.
- (87) Merzel, F.; Smith, J. C. Is the first hydration shell of lysozyme of higher density than bulk water? *Proc. Natl. Acad. Sci. U.S.A.* **2002**, *99*, 5378–5383.
- (88) Bagchi, B. Water dynamics in the hydration layer around proteins and micelles. *Chem. Rev.* **2005**, *105*, 3197–3219.
- (89) Avramov, I.; Keding, R.; Rüssel, C.; Kranold, R. Precipitate particle size distribution in rigid and floppy networks. *J. Non-Cryst. Solids* **2000**, *278*, 13–18.
- (90) McKenzie, M. E.; Deng, B.; Van Hoesen, D.; Xia, X.; Baker, D. E.; Rezikyan, A.; Youngman, R. E.; Kelton, K. Nucleation pathways in barium silicate glasses. *Sci. Rep.* **2021**, *11*, No. 69.
- (91) Yamazaki, T.; Van Driessche, A. E.; Kimura, Y. High mobility of lattice molecules and defects during the early stage of protein crystallization. *Soft Matter* **2020**, *16*, 1955–1960.
- (92) Sehnal, D.; Bittrich, S.; Deshpande, M.; Svobodová, R.; Berka, K.; Bazgier, V.; Velankar, S.; Burley, S. K.; Koča, J.; Rose, A. S. Mol*Viewer: modern web app for 3D visualization and analysis of large biomolecular structures. *Nucleic Acids Res.* **2021**, *49*, W431–W47.